THE ASTROPHYSICAL JOURNAL, 457:382–389, 1996 January 20

DETERMINATIONS OF METAL ABUNDANCES FROM *ROSAT* OBSERVATIONS

FRANZ BAUER AND JOEL N. BREGMAN
Department of Astronomy, University of Michigan, Ann Arbor, 48109;
bauer@astro.lsa.umich.edu, jbregman@astro.lsa.umich.edu
Received 1995 June 30; accepted 1995 July 28

ABSTRACT

Metallicities of thermal plasmas in the temperature range 1–30 × 10^6 K can formally be determined by spectral fitting of data from the Position Sensitive Proportional Counter (PSPC) on *ROSAT*. For the *ROSAT* band, iron is the dominant species in the metallicity determination. We examined the accuracy of PSPC abundance determinations by analyzing X-ray spectra of stars with known photospheric metallicities; coronal abundances are known for Capella from prior X-ray and extreme ultraviolet data. Metallicities are determined for 10 stars from PSPC spectra, with best-fit values equal to or less than 0.2 of the solar value, despite the fact that the known metallicities are typically near the solar value. This factor of 5 discrepancy between the known metallicities and the PSPC values is probably not due to systematically low chromospheric abundances or to instrumental miscalibration, although additional calibration tests may be warranted. Overestimation of the rate coefficients for electron-impact excitation of the Fe L lines could cause this metallicity discrepancy, so improved rate calculations would be valuable.

In spectral fits to PSPC data, the derived values for the Galactic absorption column and the X-ray temperature depend upon the adopted metallicity. Lowering the metallicity from the solar value to 0.2 of the solar value can increase the absorption column and the X-ray temperature by as much as factors of 2 and 1.5, respectively.

Subject headings: stars: abundances — stars: coronae — X-rays: stars

1. INTRODUCTION

The *ROSAT* X-ray Telescope and Position Sensitive Proportional Counter (henceforth, PSPC; see Trümper et al. 1991 for a thorough description) has permitted the study of many basic properties of thermal emitting plasmas, such as temperatures and emission measures. As the *ROSAT* mission progressed, it was understood that the PSPC had sufficient resolution to allow a determination of the metal abundance of a thermal plasma in a limited temperature range, approximately 0.2–2 keV. At those temperatures, most of the flux is carried by a multitude of emission lines, generally of Fe (also, O and N), which are unresolved and appear as a continuum. Changes in the metallicity modifies the shape of this continuum in certain areas (e.g., near 1 keV) and such effects are detectable to the PSPC, given adequate signal.

This capability of determining the metallicities has permitted investigators to examine this property in a variety of astronomical objects, often for the first time (Mulchaey et al. 1993; David et al. 1994; it can be impossible to find a unique metallicity for some spectra, as discussed in Appendix B of Trinchieri et al. 1994). In some cases, the metallicity determinations have been surprising, such as in elliptical galaxies, where the metallicity in the hot gas may formally be fitted best with a value near 0.2 of the solar value, even though the mean metallicity of the stars is near the solar value (Saracco & Ciliegi 1995; also see the X-ray abundance determination for the central 1′ in NGC 4636; Trinchieri et al. 1994; we see a similar trend in our recently obtained PSPC spectra; optical metallicities in Worthey 1994).

These low metallicities have motivated us to examine the reliability with which such quantities can be determined from PSPC data. To conduct this evaluation, we have used observations of normal stars with high-quality PSPC observations (e.g., not the luminous high- or low-mass X-ray binaries) and whose photospheric metallicities are known from optical studies (§ 2). For these stars, we examine whether the known metallicities can be recovered from the X-ray data (§ 3). For those cases where the X-rays and optical metallicities are significantly different, explanations for the differences are considered (§§ 4–5). Finally, we comment upon the implications of the metallicity problem upon spectrally determined temperatures and absorption columns (§ 6).

2. SAMPLE DEFINITION

We seek a sample of objects with known optical metallicities that can be used as "standards" to compare against X-ray inferred metallicities. To assemble our sample, we exclude the close binary systems that produce the luminous low-mass X-ray binaries and high-mass X-ray binaries (LMXB and HMXB). These systems may have several different emission processes of comparable importance, so modeling of these objects requires many parameters and may lead to ambiguous results. Instead, we primarily use late-type stars (types F–K), whose soft X-ray emission is produced in stellar coronae. Work on such systems indicates that the soft X-ray emission should be optically thin with near-equilibrium ionization conditions, and that the emission measure may be dominated by a single-temperature component (Mewe 1991; Schrijver, van der Oord, & Mewe 1994; Dupree et al. 1994). In addition, we study a few early-type stars, where the X-ray emission is thought to be produced in a stellar wind.

One of the selection criteria is that the stars were available from the *ROSAT* PSPC observational archive as of 1994 August. From the possible fields for stellar targets, we required that target sources have measured optical photospheric abundances, as listed in the Catalogue of Stellar Abundances (Cayrel de Strobel et al. 1992). This catalog contains over 3000 entries on several hundred of the brightest stars in the sky, with

abundances for a variety of elements as well as an overall average abundance relative to the Sun.

A second criterion for inclusion in our sample is that the *ROSAT* observations have an image exposure time above 500 s and that the net number of detected counts associated with the star exceed 250 (when the object lies near the field center). This criterion was met easily, with the median number of counts for the sample being 1500 and only four stars with fewer than 700 counts. The requirement for this net counts is driven by the need to have a sufficient number of counts with which to fit a spectrum. Targets not near the central part of the instrument ($>30'$), the point spread function increases substantially and vignetting becomes important. For example, a source 45′ from the center has a full width at half-maximum about 6 times larger and luminosity lower by an order of magnitude than the same source at the center. For sources away from the center, significantly more counts were required for us to include the target in the sample.

The final sample of 23 stars is given in Table 1 with an assigned number in column (1), the common name in column (2), spectral type in column (3), apparent visual magnitude in column (4), and right ascension and declination (J2000) in columns (5) through (10), as listed in SIMBAD. The image number in the *ROSAT* archive is given in column (11), the angle in minutes of arc between the position of the source and the center of the image in column (12), the useful exposure time of the image in kiloseconds in column (13), and the net number of source counts in column (14).

3. SPECTRAL ANALYSIS AND METALLICITY DETERMINATIONS

Data processing was carried out with the Post-Reduction Off-line Software (PROS, version 2.3.1), which runs under NOAO's Image Reduction and Analysis Facility (IRAF, version 2.10.2), and with the X-ray spectral package XSPEC (version 8.50), which is part of the XANADU suite of programs.

A spectrum is extracted for each star, from which we determine the likely range of metallicities, along with information about the gas temperature and the amount of intervening absorption. In obtaining a spectrum, we used a circular aperture that encompassed typically 96% of the net counts (the on-axis aperture had a typical radius of 80″). The point spread function is energy-dependent, with the greatest scattering of photons at the high-energy end of the telescope response (2 keV). We performed tests with on-axis and off-axis sources to determine if spectral fits changed when the aperture size was increased, but no substantial changes to the spectral fits were found.

For the production of a net spectrum, we removed a background spectrum from the same area and off-axis angle as the source, with all nearby point sources removed. This ensured that there was no differential vignetting between the object and background. The program "qpspec," from the PROS spectral package, was used to process source and background information and extract spectral data for use with the spectral packages. Channels 1–2 were ignored to eliminate erratic fluctuations that lead to certain kinds of systematic errors. The program XSPEC is more versatile and interactive than PROS's internal spectral package, although they give similar results, and is thus preferred for spectral fitting and plotting. The most apparent advantage is that XSPEC's interface allows the components of a fit to be monitored in more detail and gives a wider range of abundance values. It also seems to have a better, more reliable fitting routine (spectral fits in PROS sometimes became trapped in local minima).

All stars in the sample were fitted to both single and double temperature thermal spectra (Raymond & Smith 1977) with a hydrogen column density model being part of the fit; the opacity model of Morrison & McCammon (1983) was used.

TABLE 1

SAMPLE STARS

Number (1)	Name (2)	Spectral Type (3)	Apparent V (4)	R.A. 2000 (h) (5)	(m) (6)	(s) (7)	Decl. 2000 (°) (8)	(′) (9)	(″) (10)	Image Number (11)	Angle Off-Axis (arcminutes) (12)	Exposure Time (ks) (13)	Total Number of Counts (10^3 photons) (14)
1.....	δ And	K3 III	3.28	00	39	19.09	30	51	44.08	RP201045	0.30	28.37	1.48
2.....	HD 23194	A5 V	8.05	03	44	00.14	24	33	27.70	RP200008	47.89	44.18	2.84
3.....	HD 23607	A7 V	8.26	03	47	19.23	24	08	23.10	RP200008	4.28	44.18	0.37
4.....	HD 23631	A2 V	7.26	03	47	24.20	24	54	55.00	RP200008	46.36	44.18	0.88
5.....	ι Aur	K3 II	2.70	04	56	59.54	33	09	58.81	WP200402	0.24	10.64	0.73
6.....	β Cam	G1 Ib-II	4.03	05	03	25.08	60	26	32.93	WP201221	0.28	4.90	0.30
7.....	Capella	G5 IIIe+	0.08	05	16	40.93	46	00	14.22	WP200799	40.73	9.51	99.24
8.....	λ Ori	O8 III	3.30	05	35	08.20	09	56	04.00	WP200200	0.42	3.66	0.72
9.....	η Lep	F1 V	3.70	05	56	24.37	−14	10	10.95	RP200907	0.15	6.98	1.96
10.....	Canopus	F0 II	−0.72	06	23	57.01	−52	41	45.55	WP200319	0.42	3.07	1.55
11.....	S Mon	O7 Ve	4.66	06	40	58.62	09	53	44.73	WP201260	2.12	9.78	0.28
12.....	Procyon	F5 IV	0.34	07	39	20.44	05	14	21.22	WP200437	0.71	4.68	16.02
13.....	σ Gem	K1 III	4.28	07	43	18.43	28	53	12.15	WP200434	0.61	4.80	43.72
14.....	Pollux	K0 IIIb	1.15	07	45	21.26	28	01	36.60	WP200175	0.33	8.84	0.69
15.....	PI 01 UMa	G1.5 Vb	5.60	08	39	11.88	65	01	11.00	WP200654	58.95	35.44	17.49
16.....	β Vir	F9 V	3.61	11	50	39.18	01	46	06.67	WP200813	0.08	7.68	3.27
17.....	31 Com	G0 IIIp	4.94	12	51	41.89	27	32	26.92	WF200798	0.22	1.83	0.78
18.....	ι Vir	F7 IV	4.10	14	16	00.85	−05	59	40.04	RP200908	0.16	3.24	2.31
19.....	α Cen B	K1 V	1.33	14	40	00.70	−60	50	38.00	WP201119	2.97	3.32	15.06
20.....	β Her	G7 IIIa	2.77	16	30	13.47	21	29	23.27	WP201228	0.24	5.59	0.75
21.....	KSI Her	G8 III	3.70	17	57	45.49	29	14	53.29	RF200972	8.57	2.34	0.99
22.....	61 Cyg	K5 V	5.21	21	06	36.85	38	42	04.85	WF200793	4.64	4.98	0.31
23.....	λ And	G8 III	3.82	23	37	32.99	46	27	50.50	WP200433	0.43	31.64	248.35

TABLE 2

SUCCESSFUL ONE-TEMPERATURE FITS

Number (1)	Name (2)	N_h (10^{20}) (3)	$T1$ (keV) (4)	Norm1 (10^{-14} cm^{-5}) (5)	X-Ray Z (6)	χ^2_ν (7)	Range in X-Ray Z at 99% Confidence Level (8)	Optical Z (9)
1.....	δ And	0.000	0.500	0.00048	0.05	0.391	0.0–0.4	1.02
2.....	HD 23194	2.549	0.729	0.00140	0.06	0.488	0.01–0.3	0.46
7.....	Capella	0.107	0.678	0.10041	0.20	3.849	0.16–0.22	1.86
9.....	η Lep	0.000	0.371	0.00241	0.10	0.932	0.02–0.45	0.44
10.....	Canopus	0.848	0.604	0.00556	0.10	0.347	0.05–0.6	0.86
13.....	σ Gem	0.357	0.935	0.07726	0.20	2.867	0.12–0.25	0.50
15.....	PI 01 UMa	0.000	0.392	0.00543	0.15	2.393	0.1–0.2	0.50
16.....	β Vir	0.000	0.331	0.00417	0.07	0.933	0.01–0.2	0.20
18.....	ι Vir	0.436	0.595	0.00577	0.15	0.510	0.05–0.45	0.76
23.....	λ And	0.401	0.849	0.07797	0.10	14.840	0.09–0.12	0.20

For several of the stars, the absorption column was negligibly small and played no role in the spectral fit. For certain stars, such as those in the Pleiades or Hyades, the absorption column can be estimated from other studies (e.g., Table 3 in Mewe 1991), although the column varies in an irregular fashion over these star clusters (e.g., inspect the Palomar Sky Survey).

For each star, a series of models were fitted for a sequence of values of the metallicity (Z). That is, a value of the metallicity was held fixed and the temperature(s), emissivity, and absorption column were fitted. The metallicities were varied from 0.01–0.1 of the solar value to 3–4 times the solar value. Each fit is characterized by a value of the reduced χ^2 (henceforth, χ^2_ν) so this analysis leads to χ^2_ν as a function of metallicity. The deviation of χ^2_ν from its minimum value permits us to define allowable values of the metallicity to some adopted level of confidence.

Most of the stars were suitably fitted with a single-temperature plasma in that the addition of a second temperature component did not significantly reduce the χ^2_ν. From this sample, the spectra of 10 stars were sensitive to changes in the metallicity (generally, those stars with the most counts; Table 2). For the metallicity to be considered well determined, the range in χ^2_ν values among the models must change by a significant amount so most of the metallicity range is excluded at the 99% confidence level. The best-fit spectral parameters are given in Table 2 (cols. [3]–[6]), along with the corresponding χ^2_ν (col. [7]), the allowed range of the metallicity (col. [8]), and the known optical metallicity (col. [9]).

For three stars, there were sufficient counts that the metallicity could be constrained when using a two-temperature fit, and the results are presented in Table 3. The addition of a second temperature significantly decreased the χ^2_ν for σ Gem and for λ And, but led only to a modest decrease in χ^2_ν for Capella. The addition of a second temperature component did not change the best-fit value for the metallicity in Capella or in σ Gem, but it did cause a modest increase in the best-fit metallicity for λ And (from 0.06 to 0.10). The χ^2_ν value for the spectral fit (col. [9], Table 3) seems higher than expected for an acceptable fit, but is largely due to the uncertainties in the calibration, which are at the level of a few percent (Snowden et al. 1995). This miscalibration becomes important only when the uncertainty from photon noise is lower than the calibration error, as is the case here.

Whenever the fitting restricted the metallicity to a narrow range, the best-fit value was always less than or equal to 0.2 of the solar value. This was nearly always less than the solar photospheric value, and typically is lower by an order of magnitude (Tables 2, 3; Fig. 1, 2). *The X-ray determinations for the metallicity appear to be systematically lower than their photospheric values by a large amount.*

4. CAPELLA AS A CASE STUDY

Capella is a well-studied multiple star system primarily composed of a G5 III star and a F9 III star in which the stars are sufficiently separated that the soft X-rays seen are produced in their separate coronae rather than through an accretion or interaction region. Coronal properties of Capella A and B have been studied by observations in the ultraviolet (Ayres 1988), the extreme ultraviolet (Dupree et al. 1994), and the soft X-rays (Holt et al. 1979; Swank et al. 1981; Vetter & Canizares 1983; Lemen et al. 1989). It has an optical photospheric mean abundance of 1.9 times solar (Mercki, Strobel, & Strobel 1986).

Previous soft X-ray observations with the Focal Plane Crystal Spectrometer on the *Einstein Observatory* (Vetter & Canizares 1983) indicated that the spectrum could be modeled with a dominant single-temperature plasma at 6.3×10^6 K (0.54 keV) at the solar abundance. Their fit to the spectrum was improved slightly when the iron abundance was increased to twice the solar value, which is approximately the photospheric abundance; their observation was not particularly sensitive to higher temperature gas. Observations with the Solid State Spectrograph on the *Einstein Observatory* have much poorer spectral resolution but much broader energy coverage (Holt et al. 1979; Swank et al. 1981; J. H. Swank, private

TABLE 3

SUCCESSFUL TWO-TEMPERATURE FITS

Number	Name	N_h (10^{20})	$T1$ (keV)	Norm1 (10^{-14} cm^{-5})	$T2$ (keV)	Norm2 (10^{-14} cm^{-5})	X-Ray Z	χ^2_ν	Range in X-Ray Z at 99% Confidence Level	Optical Z
7.....	Capella	0.140	0.130	0.00264	0.680	0.09990	0.20	3.391	0.15–0.3	1.86
13.....	σ Gem	0.312	0.844	0.05320	2.006	0.02260	0.20	1.587	0.15–0.4	0.50
23.....	λ And	3.630	0.017	645.90	0.788	0.10800	0.06	4.411	0.05–0.06	0.20

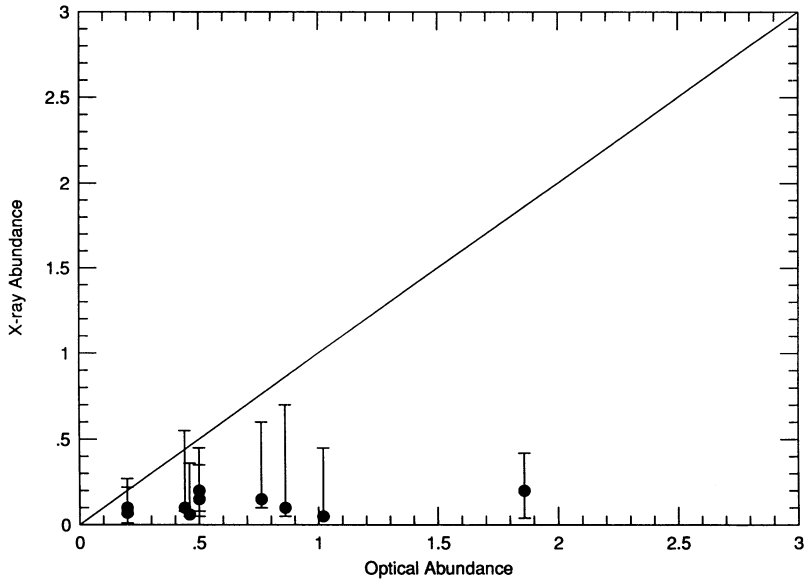

FIG. 1.—Metallicities as derived from one-temperature spectral fits to PSPC X-ray data vs. the optical photospheric abundances. The best-fit X-ray metallicities, which are less than or equal to 0.2 of the solar value, do not increase with the optical photospheric abundance and are typically a factor of 5 lower. A linear correlation line is shown for comparison.

communications), and these data require a two-temperature fit with temperatures of 4.5×10^6 K (0.39 keV) and 1.3×10^7 K (1.1 keV). An abundance of about twice the solar value is indicated, consistent with the photospheric value. A two-temperature model is also necessary to fit the *EXOSAT* data, with temperatures of 4.7×10^6 K (0.40 keV) and 2.2×10^7 K (1.9 keV; Lemen et al. 1989).

High spectral resolution observations of the very soft X-ray region have been obtained by the *Extreme Ultraviolet Explorer* satellite (*EUVE*; 0.5–2.0 Å resolution over the range 75–360 Å), revealing many iron lines as well as oxygen, nickel, magnesium, and helium lines (Dupree et al. 1993; Brickhouse 1995). These coronal observations reveal a continuous distribution of emission measure with temperature up to 2×10^7 K, although there is a strong peak at 6×10^6 K (0.52 keV). These *EUVE* observations indicate that the iron abundance is near the solar value (0.88 ± 0.13 of the solar value; Brickhouse 1995), as is sulfur, while nickel and silicon are about twice the solar value, and oxygen is in the range 0.4–1.0 of the solar value.

Modest spectral resolution X-ray spectra have recently been obtained by *ASCA*, and abundance determinations are reported in Drake et al. (1994), although details of the analysis are to be published at a future date. These abundances are lower than, and in some cases, inconsistent with the above authors,

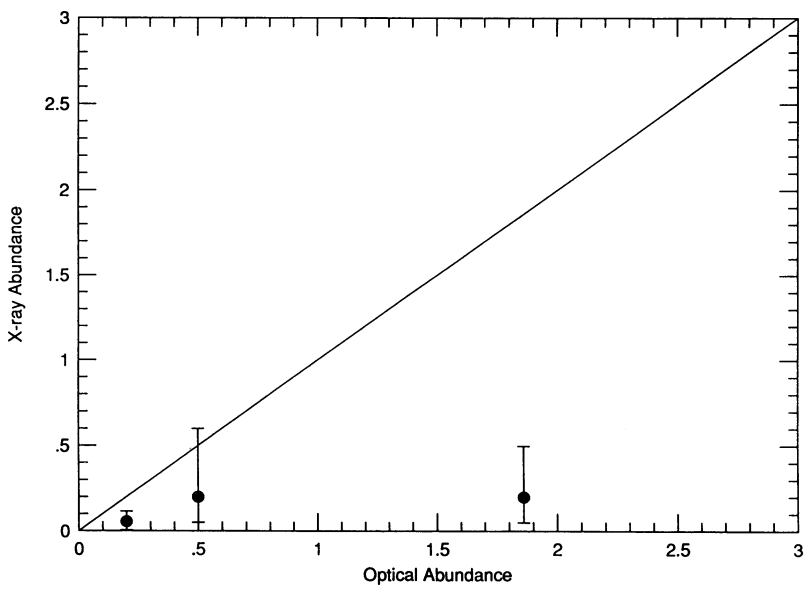

FIG. 2.—For stars with a large number of counts, metallicities are derived from two-temperature spectral fits to PSPC X-ray data and compared to the optical photospheric abundances. The best-fit X-ray metallicities are 2.5–9 times smaller than the optical abundances and there is no correlation between the two metallicities. A linear correlation line is shown for comparison.

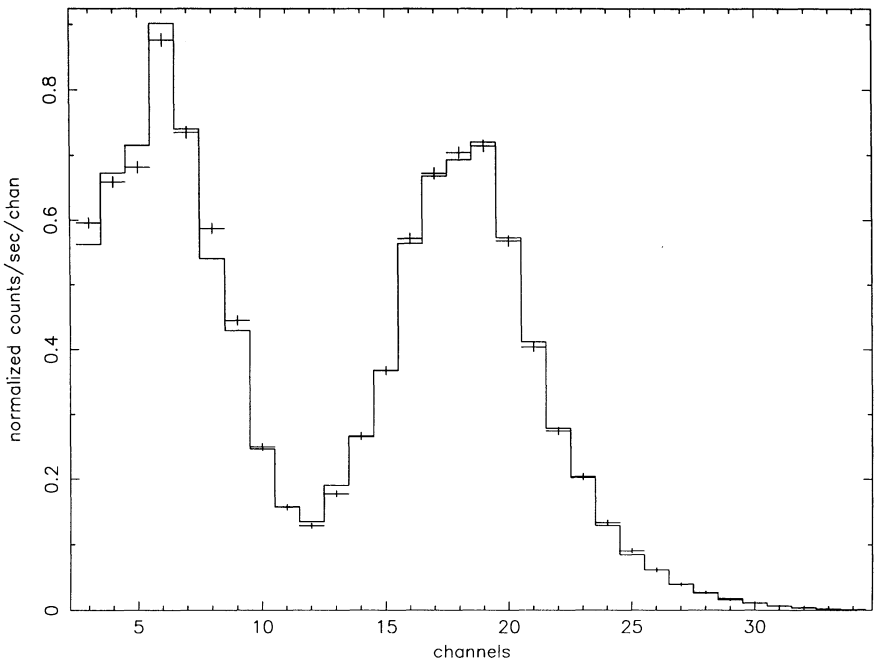

FIG. 3*a*

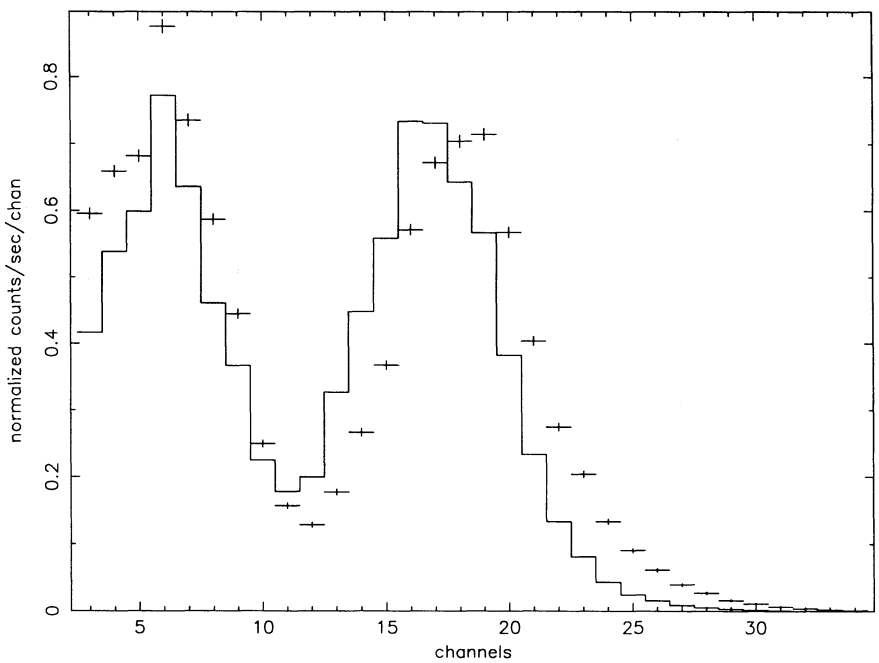

FIG. 3*b*

FIG. 3.—The count rate per channel for Capella (*crosses*) over the PSPC band and the best-fit single-temperature spectrum (*solid line*). The channels correspond to a band energy where the median energies are 0.125 keV for channel 3, 0.22 keV for channel 6 (the first peak), 0.50 keV for channel 12 (the local minimum), 1.03 keV for channel 19 (the second maximum), 1.45 keV for channel 25, and 1.96 keV for channel 30. The most successful fit (*panel a*) occurs for a metallicity of 0.20 of the solar value and a temperature of 0.68 keV (Table 2). When the metallicity is fixed at 1.9 of the solar value, which is the photospheric metallicity, no acceptable fit is found, with a minimum $\chi^2_\nu = 317$ (*panel b*); the temperature is 0.31 keV and $N_H = 0$.

with an Fe abundance of 0.46 (−0.36, +0.61) solar, and an O abundance of 0.13 (−0.03, +0.27) solar. We note that the *ASCA* spectra do not resolve the line complexes.

From our *ROSAT* data, the best-fit one-temperature thermal plasma model has a temperature of 7.9×10^6 K (0.68 keV; metallicity of 0.2 solar; Table 2; Fig. 3*a*), about 20% hotter than the *Einstein Observatory* FPCS temperature or the dominant component seen by the *EUVE*. When we require a best-fit from a thermal plasma with the photospheric abundance (1.9 times solar), the fit is clearly unacceptable (Fig. 3*b*), with $\chi^2_\nu = 317$ (even permitting $N_{HI} = 0$).

Two-temperature plasma models lead to the same dominant temperature component at 7.9×10^6 K (0.68 keV) and another less significant component at 1.5×10^6 K (0.13 keV; Table 3),

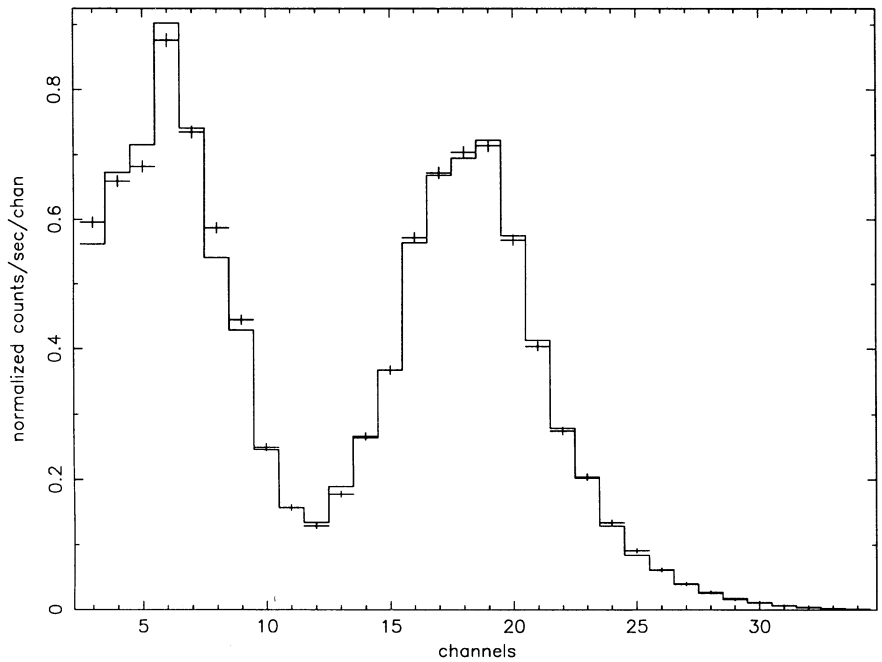

FIG. 4*a*

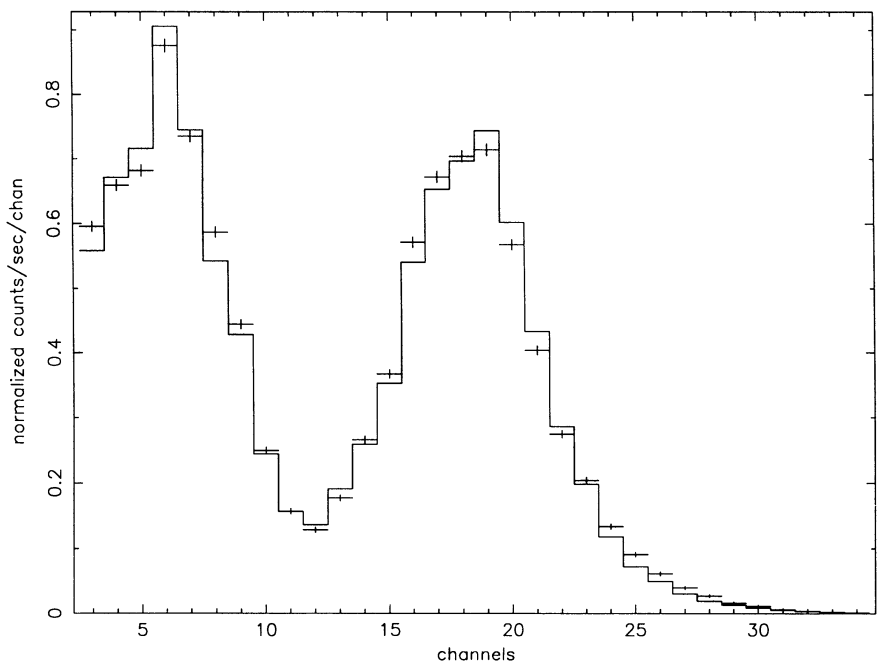

FIG. 4*b*

FIG. 4.—The count rate per channel for Capella (*crosses*) over the PSPC band and the best-fit two-temperature spectrum (*solid line*). The channel energies are the same as those given for Fig. 3. The best-fit (*panel a*) requires a metallicity that is 0.20 of the solar value and the spectrum is very similar to the single-temperature fit of Fig. 3*a* (spectral fit properties given in Table 3). When the metallicity is fixed at 1.9 of the solar value, the minimum χ_ν^2 indicates that the fit is not acceptable (*panel b*). For the high-metallicity fit, the two temperatures are 0.148 keV and 0.767 keV, the ratios of the emission measure for these two components is 0.52, $N_H = 1.7 \times 10^{19}$ cm^{-2}, and $\chi_\nu^2 = 9.97$.

with a modest decrease in χ_ν^2 compared to the one-temperature fits (Fig. 4*a*). The ratio of normalizations of these two temperature components is consistent with the emission measure distribution measured by the *EUVE*. With the best-fit two-temperature models, a metallicity is required of about 0.2 times the solar value, primarily driven by the iron abundance. Increasing the metallicity to the average photospheric value yields an unacceptable fit (the χ_ν^2 rises from 3.39 to 9.97), significantly changing the shape of the spectrum (Fig. 4*b*).

Additional models for the *ROSAT* data were fitted based upon the emissivity distribution given by the *EUVE* analysis (Dupree et al. 1993). Three-temperature models were investigated, with temperatures of 0.1–0.2 keV, 0.5–0.8 keV (the dominant component), and 2–3 keV (the least significant).

However, best-fit models still required values for the metallicity near 0.2 of the solar value.

Another set of models was calculated where we adopted the abundance determinations from the *ASCA* and *EUVE* satellites (separately) and then searched for the best one-temperature and two-temperature fits. None of these models led to acceptable fits, so we considered other models where individual abundances could be adjusted. The primary parameter in obtaining acceptable fits is the Fe abundance, with the best fit coming for an abundance near 0.2 of the solar value. Varying the other abundances had relatively little effect on the outcome.

There appears to be an irreconcilable difference between the metallicity (mainly Fe) inferred from the analysis of the *ROSAT* data and the metallicities determined for the corona with the *EUVE* or for the photosphere from ground-based observations. Although the most extensive testing was carried out for Capella, similar spectral differences to Figures 3 and 4 are found in other stars (e.g., σ Gem).

5. DISCUSSION

There are three possible explanations for the failure to recover the known metallicities by using *ROSAT* PSPC data: the PSPC may be miscalibrated, the plasma line emission model may be wrong, or the metallicity of 10^7 coronal gas may be systematically low. In considering miscalibration issues, it is necessary to realize that the instrumental response is double-peaked at 0.2 keV and 1 keV, so most spectra reflect this structure. Determinations of the metallicity depend upon the shape of each peak and of the ratio of the two. Any miscalibration that systematically changes either the shape or the relative heights of the two peaks will lead to incorrect metallicities. There are calibration inaccuracies in the PSPC typically at the level of a few percent, as discussed by Snowden et al. (1995). However, these inaccuracies do not obviously change the shape or relative height of the peaks by a substantial amount. If there were such systematic problems, they would be evident in the fitting of galactic nuclei (AGNs) spectra, which are generally represented with a single power law plus absorption column in the PSPC energy range. Fits to AGNs do not reveal systematic residuals (Laor et al. 1994), although the underlying spectrum is not known a priori. Furthermore, higher spectral resolution X-ray observations with *ASCA* are finding low metallicities for some stars (e.g., Cochran et al. 1994; Drake et al. 1994; J. L. Linsky, private communication). These arguments suggest that miscalibration of the PSPC is not the likely cause of the low metallicities found with the PSPC.

In conflict with this conclusion are the SSS observations from the *Einstein Observatory*, which covers the same energy range as *ROSAT* yet requires a metallicity equal to the photospheric metallicity, an order of magnitude greater than the metallicity determined from the PSPC. However, there have been calibration problems with the SSS due to periodic accumulation of ice in the optical path, so it remains to be proved that a calibration problem lies with the PSPC rather than with the SSS.

The second possibility is that the metallicities in the corona are significantly lower than in the photosphere. A significant difference is known for the Sun, where elements with a first ionization potential below 13.6 eV are overabundant in the corona by factors of 2–4 while species with a first ionization potential above 13.6 eV display photospheric abundances (the first ionization potential or FIP effect; e.g., McKenzie & Feldman 1992; Laming, Drake, and Widing 1995). The first ionization potential of Fe is 7.87 eV, and it has an enhanced abundance in the Solar corona, not a depleted abundance as would be necessary to understand the low *ROSAT* metallicities. This FIP effect has been studied in detail in only a few stars and it is not detected in Procyon, where the coronal abundances are consistent with their photospheric values (*EUVE* observations of Drake, Laming, & Widing 1995). The *EUVE* observations of Capella also are approximately solar for Fe (see above; Brickhouse 1995). Therefore, there is no evidence that the Fe abundances in coronae are less than in photospheres, and a coronal Fe enhancement is more likely to be the case.

The final possibility is that there is a problem with the radiative model. It is unlikely that there is a technical problem, such as a fault in the programming, since spectral fits with the radiative code developed by J. Raymond yield nearly identical results to the code developed independently by Mewe. However, it is likely that some of the atomic physics parameters used by these models are in error, such as certain Fe line collision strengths. For example, Chen & Reed (1989) calculate the resonance-excitation rate coefficients for transitions from the ground state to the $2p^5 3s$ excited state in Fe XVII, and at temperatures (0.20 keV) below where the rate coefficients peak (0.5–1 keV), their coefficients are 3–5 times smaller than those calculated by Smith et al. (1985; for a recent review of collision strengths, see Lang 1994, and especially Badnell & Moores 1994). A reduction in the Fe line collision strengths would lead to larger inferred abundances of Fe, although the magnitude of this abundance increase remains unclear. In light of the disagreement in certain Fe electron-impact excitation rates, improvements in the determination of these rates would be most welcome, followed by their implementation in the radiative codes used for X-ray spectral analysis.

6. IMPLICATIONS AND FINAL REMARKS

While this work casts doubt on the validity of metal abundances as obtained from the PSPC, it is ncessary for workers in the field to choose a value of the metallicity in order to carry out spectral analysis of *ROSAT* data with thermal plasmas. When using a Raymond-Smith plasma, the choice of metallicity affects the values deduced for the temperature and the absorption column. For a single-temperature model, lowering the metallicity from the solar value to 0.2 of the solar value leads to an average increase in the inferred $N_{\rm H}$ by a factor of 2 (for $N_{\rm H} \approx 1\text{–}5 \times 10^{20}$ cm^{-2}) and an average increase in the temperature by 1.5. In a few objects that we have examined, the spectral fitting procedure arrives at the Galactic value of $N_{\rm H}$ when a metallicity near 0.5 of the solar value was adopted.

We have studied whether the excess absorption seen toward the centers of clusters of galaxies is a reflection of a change in the metallicity rather than in the absorption. For high-temperature plasmas, such as that given by the mean cluster temperatures, changes in the metallicity have little effect on the determination of $N_{\rm H}$. This is expected, since at temperatures of 4–10 keV, the dominant emission mechanism is free-free radiation, which is insensitive to the metallicity. At lower temperatures, metallicity effects can play a role, and if the true abundance gradient in the cluster is shallower than assumed (or inverted), it would be possible to decrease or avoid excess absorption in a cluster center. Although inverted abundance gradients seem unlikely, investigators might care to vary the

abundances to determine the effect in these particular situations.

We would like to thank John Raymond, Nancy Brickhouse, Jeff Linsky, Jean Swank, Craig Sarazin, Steve Snowden, Dick Teske, Tim Heckman, Trevor Ponman, Wolfgang Pietsch, Charles Cowley, Larry David, Christine Jones, Bill Forman, and Pepi Fabbiano for their advice, suggestions, and the release of material prior to publication. Also, we wish to acknowledge a valuable referee's report from Francis Keenan, whose advice on Fe collision line strengths was particularly timely. We are grateful for the extensive use of "classic" ADS database software and the SIMBAD database, operated at CDS, Strasbourg, France. Support for this research was provided by NASA through grants NAGW-2135 and NAG 5-1955.

REFERENCES

Ayres, T. R. 1988, ApJ, 331, 467
Badnell, N. R., & Moores, D. L. 1994, Atomic Data Nucl. Data Tables, 57, 329
Brickhouse, N. S. 1995, in IAU Coloq. 152 Astrophysics in the Extreme Ultraviolet (Cambridge: Cambridge University Press), in press
Cayrel de Strobel, G., Hauck, B., Francois, P., Thevenin, E., Friel, E., Mermilliod, M., & Borde, S. 1992, A&AS, 95, 336
Chen, M. H., & Reed, K. J. 1989, Phys. Rev. A, 40, 2292
Corcoran, M. F., et al. 1994, ApJ, 436, L95
David, L. P., Jones, C., Forman, W., & Daines, S. 1994, ApJ, 428, 544
Drake, S. A., Laming, J. M., & Widing, K. G. 1995, ApJ, 443, 393
Drake, S. A., Singh, K. P., White, N. E., & Simon, T. 1994, ApJ, 436, L87
Dupree, A. K., Brickhouse, N. S., Doschek, G. A., Green, J. C., & Raymond, J. C. 1993, ApJ, 418, L41
Dupree, A. K., Hartmann, L., Smith, G. H., Rodgers, A. W., Roberts, W. H., & Zucker, D. B. 1994, ApJ, 421, 542
Holt, S. S., White, N. E., Becker, R. H., Boldt, E. A., Mushotzky, R. F., Serlemitsos, P. J., & Smith, B. W. 1979, ApJ, 234, L65
Laming, J. M., Drake, J. J., & Widing, K. G. 1995, ApJ, 443, 416
Lang, J. 1994, Atomic Data & Nucl. Data Tables, 57, 1
Laor, A., Fiore, F., Elvis, M., Wilkes, B. J., & McDowell, J. C. 1994, ApJ, 435, 611
Lemen, J. R., Mewe, R., Schrijver, C. J., & Fludra, A. 1989, ApJ, 341, 474
McKenzie, D. L., & Feldman, U. 1992, ApJ, 389, 764
Mewe, R. 1991, A&AR, 3, 127
Morrison, R., & McCammon, D. 1983, ApJ, 270, 119
Mulchaey, J. S., Davis, D. S., Mushotzky, R. F., & Burstein, D. 1993, ApJ, 404, L9
Raymond, J., & Smith, B. 1977, ApJS, 35, 419
Saracco, P., & Ciliegi, P. 1995, A&A, in press
Schrijver, C., van der Oord, G., & Mewe, R. 1994, A&A, 289, L23
Smith, B. W., Raymond, J. C., Mann, J. B., & Cowan, R. D. 1985, ApJ, 298, 898
Snowden, S. L., Turner, T. J., George, I. M., Yusaf, R., Predehl, P., & Prieto, A. 1995, OGIP Calibration Memo CAL/ROS/95-003
Stauffer, J. R., Caillault, J. P., Gagne, M., Prosser, C. F., & Hartmann, L. W. 1994, ApJS, 91, 625
Swank, J. H., White, N. E., Holt, S. S., & Becker, R. H. 1981, ApJ, 246, 208
Trinchieri, G., Kim, D.-W., Fabbiano, G., & Canizares, C. R. C. 1994, ApJ, 428, 555
Trumper, J., et al. 1991, Nature, 349, 579
Vedder, P. W., & Canizares, C. R. 1983, ApJ, 270, 666
Worthey, G. 1994, ApJS, 95, 107